Journal of Marine Systems 140 (2014) 50–58

Contents lists available at ScienceDirect

Journal of Marine Systems

journal homepage: www.elsevier.com/locate/jmarsys

Cyanobacterial bloom detection based on coherence between ferrybox observations

Philipp M.M. Groetsch [a,b,c,*], Stefan G.H. Simis [d], Marieke A. Eleveld [b], Steef W.M. Peters [c,b]

[a] Tartu Observatory, 61602, Tõravere, Estonia
[b] VU University Amsterdam, Institute for Environmental Studies (IVM), De Boelelaan 1087, 1081 HV Amsterdam, The Netherlands
[c] Water Insight, Marijkeweg 22, 6709 PG Wageningen, The Netherlands
[d] Finnish Environment Institute SYKE, Erik Palménin Aukio 1, 00560 Helsinki, Finland

ARTICLE INFO

Article history:
Received 31 August 2013
Received in revised form 28 March 2014
Accepted 22 May 2014
Available online 4 June 2014

Keywords:
Ferrybox
Remote sensing
Cyanobacteria
Bloom
Stratification
Spatial variability
Data assimilation
Wavelets
Baltic Sea

ABSTRACT

Cyanobacterial bloom detection from flow-through optical sensors on ships-of-opportunity ('ferryboxes') is challenging in periods of strong stratification and due to varying cell physiology and phytoplankton community composition. Wavelet coherence analysis between ferrybox parameters (chlorophyll-*a* fluorescence, phycocyanin fluorescence, turbidity) was used to delineate blooms in a dataset of ten ferrybox transects, recorded during the 2005 cyanobacterial bloom season in the Baltic Sea. Independent wind speed and sea-surface temperature data were used to classify areas of cyanobacterial dominance as mixed, stratified, or surfacing bloom. These classified subsets of ferrybox observations were compared against remotely sensed chlorophyll-*a* concentrations, which resulted in a scheme for the interpretation of surface water phytoplankton biomass from multi-source observations. Ferrybox optical signals were significantly coherent from the onset until the end of the cyanobacterial bloom period under both stratified and mixed conditions. This suggests that the coherence analysis is sensitive to high-level community composition. Strongly stratified and suspected surfacing bloom was associated with unrealistically high remotely sensed chlorophyll-*a* estimates, indicating the need to flag stratified bloom areas when interpreting remote sensing imagery. The ferrybox fluorescence and turbidity signals at the 5-m sampling depth were, paradoxically, low under these conditions, suggesting that direct comparison between remote sensing and flow-through observations is not useful for stratified blooms. Correlations between ferrybox measurements and remotely sensed observations improved consistently when stratified or surfacing cyanobacterial bloom was excluded from the regression.
It is discussed how coherence analysis of ferrybox observations can aid the interpretation of remotely sensed data in situations where meteorological observations suggest incomplete vertical mixing.

1. Introduction

Detection and quantification of phytoplankton blooms are essential to understand their role in biogeochemical cycling and to manage the economical and health impacts of harmful species (Anderson, 1997; Carstensen et al., 2004). Increase in bloom duration and intensity can indicate eutrophication (Anderson et al., 2002; Hallegraeff, 1993; Heisler et al., 2008) and is increasingly used in the context of climate change research (e.g. Gnanadesikan and Anderson, 2009; Paerl and Huisman, 2009). Blooms are target for monitoring due to potential accumulation of toxin-producing species and their ecosystem-destabilizing effects (Hansson and Hakansson, 2007). Reliable observations of phytoplankton blooms with high spatiotemporal coverage are prerequisite to produce bloom metrics. Remote sensing techniques have been successfully applied in this context in the open oceans, whereas the optical complexity of coastal waters calls for a combined use of remote sensing and *in situ* observation techniques. The high spatial and temporal resolution of *in situ* measurements with flow-through optical sensors on ships-of-opportunity ('ferryboxes') theoretically supports assimilation with optical remote sensing measurements. The resulting synoptic information is essential for coastal management and risk assessment (Pulliainen et al., 2004; Vepsäläinen et al., 2005).

Fluorescence from the main photosynthetic pigment chlorophyll-*a* (CHLa) is the most common biological parameter measured from ferryboxes and is used as a proxy for phytoplankton biomass (Campbell and Hurry, 1998; Kiefer, 1973). Fluorescence observations are non-ideal proxies of surface water phytoplankton biomass, due to cell physiological variability (nutrient and light adaptation, including diurnal cycles), as well as variable phytoplankton group composition (Campbell and Hurry, 1998). Ferrybox parameters may be calibrated against bottle samples analyzed in the laboratory, to overcome some of this variability. Such procedures may or may not reconcile the fundamentally different optical signals measured with fluorescence sensors at the ferrybox intake depth

* Corresponding author at: Water Insight, Marijkeweg 22, 6709 PG Wageningen, The Netherlands.

http://dx.doi.org/10.1016/j.jmarsys.2014.05.015

(3–5 m) and remotely sensed reflectance (representing the first optical depth, Gordon and McCluney, 1974). As long as the mixing depth exceeds the first optical depth both, remotely sensed and ferrybox observations of phytoplankton biomass, can be seen as representative of surface layer processes. However, the variable response between remote and *in situ* optical sensors of choice must be taken into account in monitoring practices, particularly in situations where steep vertical gradients in light and nutrient availability are expected, such as is the case during phytoplankton bloom.

Some of the clearest examples of discrepancies between *in situ* and remotely sensed observations are for blooms of motile or buoyant cyanobacterial species (Walsby et al., 1997) under prevalent calm wind conditions (Kanoshina et al., 2003; Wynne et al., 2010). Ship-induced mixing may or may not break such stratified layers (Kanoshina et al., 2003), whereas remote sensing observations will always represent the first optical depth. Optical remote sensing does not provide information about the degree of vertical mixing, hence algorithms for the retrieval of water constituent concentrations from remote sensing imagery assume vertically mixed water columns. Kutser et al. (2008) simulated remote sensing reflectance for various concentration-depth profiles found under bloom conditions, concluding that large errors in the concentration retrieval can result from the wrong assumption of mixing depth. Therefore, neither remote sensing nor ferrybox observations are expected to yield consistently reliable estimates of cyanobacterial biomass in highly stratified situations. Consequently, unknown mixing conditions are accepted as a source of uncertainty in most approaches for the assimilation of ferrybox and remote sensing data (e.g. Pulliainen et al., 2004).

In this study, we explore the spatial variability of high-frequency ferrybox optical signals as a means to identify cyanobacteria-dominated sections of ferrybox transects. We hypothesize that coherence between signals will be less sensitive to stratification compared to the interpretation of signal magnitude as an indicator for bloom conditions. Including signal coherence and stratification in the interpretation and assimilation of multi-source observation data can then lead to more robust monitoring practices.

In the last decade, Baltic Sea ferrybox systems have been increasingly equipped with phycocyanin (PC) fluorescence sensors to record regularly occurring cyanobacterial summer blooms (Kahru et al., 2007). PC is the major phycobilipigment in the filamentous cyanobacteria that frequently dominate these blooms. Seppälä et al. (2007) observed that a combination of PC and CHLa fluorescence serves as a better proxy of extracted CHLa than CHLa fluorescence alone, due to the different expression of CHLa fluorescence in cyanobacteria compared to algae (Johnsen and Sakshaug, 1996). Hence, CHLa fluorescence and PC fluorescence are expected to vary coherently in cyanobacterial blooms. Bloom-forming cyanobacteria are often efficient light scatterers (colony formation, gas vesicles), so signal coherence between turbidity (a light scattering measurement) and PC fluorescence may also be expected under bloom conditions.

To determine spatial coherence in transect data we must look beyond analytical techniques that determine the correlation between two stationary signals whose statistical parameters such as mean or variance do not change in time or space. Here, we select wavelet coherence analysis to overcome this restriction and to simultaneously resolve changes in the coherence between signals in the spatial dimension. Wavelet coherence is based on continuous wavelet transform (CWT), an analytical technique that resolves changes in the frequency distribution of a given signal. In a wavelet coherence analysis, two wavelet-transformed signals are compared, exposing locations and scales of coherent variation. In contrast to short-time Fourier transform or windowed cross-correlation, CWT and wavelet coherence require no arbitrary choice for window sizes and associated spatial/temporal resolution. CWT has been used independently and in conjunction with wavelet coherence analysis to examine frequency and scaling properties of non-stationary data in various disciplines, including phytoplankton ecology (Blauw et al., 2012) and water remote sensing (Ampe et al., 2013).

The present study applies wavelet coherence analysis to ferrybox data from the summer bloom period of 2005 in the Baltic Sea, when frequent surfacing of cyanobacteria biomass was observed. Ferrybox fluorescence of CHLa and PC, as well as turbidity is submitted to wavelet coherence analysis. Sea-surface temperature (SST) and wind speed are used as independent indicators of potentially stratified conditions. Kahru et al. (1993) previously demonstrated that elevated SST can be associated with surface-accumulated cyanobacteria, while George and Edwards (1976), Hunter et al. (2008) and Wynne et al. (2010) found that wind-induced mixing dissipates stratified surface layers for wind speeds exceeding 4–7.7 ms^{-1}.

Following the wavelet coherence interpretation of ferrybox transect data, we asses whether the method provides a consistent delineation of the cyanobacterial bloom. Automated platforms on ships-of-opportunity do not provide the means for independent validation of mixing depth, and offer only sparse documentation of community composition. Hence, we focus on a corroborating interpretation of the seasonal succession of the phytoplankton from ferrybox and meteorological observations. Further evidence of an improved interpretation is sought by comparing the bloom-delineated transects against CHLa interpreted from remote sensing imagery of the area, treating stratified and surfacing bloom areas separately from well-mixed situations.

The presented scheme is intended to improve exploitation of remote and *in situ* observation sources to provide better estimates of column biomass for models of primary production, (surface) bloom occurrence for risk assessment, as well as mixing depth for the interpretation of spatiotemporal trends in observed biomass.

2. Materials and methods

2.1. Input data

Average wind speed (longitudinal and latitudinal components) and sea surface temperature were extracted from the ECMWF Interim Reanalysis archives (Dee et al., 2011) for the period of 20 June until 31 July 2005, along the ferrybox transect in Fig. 1 and plotted in Fig. 2. These data were stored on a reduced Gaussian grid with a spatial resolution of 0.75°(≈83 km) and a temporal resolution of six hours (12 am, 6 am, 12 pm and 6 pm UTC). Spatio-temporal interpolation was carried out to match the resolution of the *in situ* data and to avoid discontinuities when extracting the variables along the ferry transect.

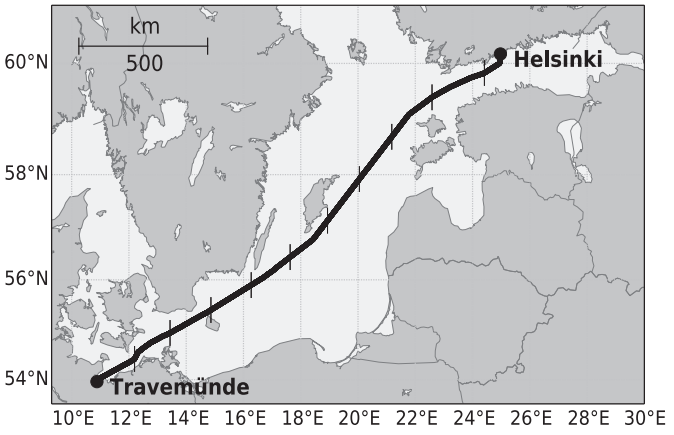

Fig. 1. Route of M/S *Finnpartner* from Travemünde (Germany) to Helsinki (Finland). Black bar-markers are drawn every 100 km along the transect.

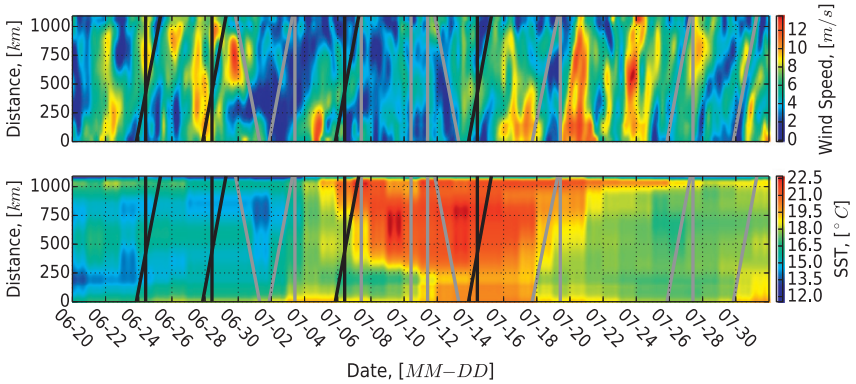

Fig. 2. ECMWF Interim reanalysis full resolution absolute wind speed (top panel) and sea surface temperature (bottom panel) along the transect in Fig. 1. The distance is measured from Travemünde, Germany (0 km) to Helsinki, Finland (1091 *km*) and the dates (MM-DD) refer to 2005. The vertical black and gray lines mark the remote sensing scene date/time and the tilted black and gray lines indicate the ship transects. Black line color indicates an *in situ*-remote sensing match-up.

For both spatial and temporal interpolation a bivariate 5th-order spline was used. Absolute wind speeds were calculated from the longitudinal and latitudinal components.

The *in situ* data used in this study were collected from the Alg@line network of Baltic Sea ferryboxes, from the route sailed by the cargo vessel M/S *Finnpartner*, which commuted between Travemünde (Germany) and Helsinki (Finland) as depicted in Fig. 1. Twelve transects were recorded on that transect in the period of 23 June to 27 July 2005, two of which were omitted due to failure of one of the instruments. The system recorded in vivo fluorescence of CHLa and PC pigments as well as turbidity, salinity and temperature. Details about the instrumentation of the the Alg@line systems are given in (Leppänen et al., 1994; Rantajärvi et al., 2003; Ruokanen et al., 2003; Seppälä et al., 2007). A sampling interval of 20 s resulted in a nominal spatial resolution of 200 m, depending on ship speed. Uncalibrated fluorescence values were used for the analysis because the calibration against laboratory extracts (e.g. multiplication by a constant and adding an offset) would not influence the variability of the signal and therefore the wavelet coherence results.

Medium Resolution Imaging Spectrometer (MERIS) FR L1b data (3rd reprocessing, IPF6.0, MEGS8) with a nominal spatial resolution of 300 m were processed to CHLa concentrations using the WeW/FUB algorithm (Schroeder and Behnert, 2007; Schroeder et al., 2007), which is integrated in VISAT BEAM (V. 4.11). This algorithm is commonly used for operational monitoring of cyanobacteria in the Baltic Sea region and was validated with Baltic Sea data sets (Kratzer et al., 2008; Stelzer et al., 2008). WeW/FUB relies on a neural network, which regards the atmosphere and the water column as one physical system and therefore solves the atmospheric correction and water constituent retrieval simultaneously. CHLa concentrations along the transect in Fig. 1 were extracted from the satellite image (data shown in the last panel of Fig. 4). Gaussian blur ($\sigma = 0.5$) was applied to the image prior to the transect extraction to avoid aliasing effects and the flags provided by the WeW/FUB algorithm were used to mask invalid pixels. The ferrybox data sets covered the transect with typically 6000–7000 observations. These, and the extracted remote sensing observations were linearly interpolated to a common length of 10,000 data points to facilitate data handling and comparison efforts.

2.2. Wavelet analysis

Continuous wavelet transform (CWT) translates temporal or spatial data into the wavelet domain. Conceptually CWT is similar to a Fourier series where a signal is decomposed into sines and cosines. However, in the wavelet domain the signal is expressed with scaled and translated versions of a *mother-wavelet*. Other than sine and cosine, *mother-wavelets* are localized functions and thus changes in scaling properties within a data set can be resolved (Torrence and Compo, 1998). We used the Morlet *mother-wavelet* because its resolution of scale and location are approximately equal (Maraun and Kurths, 2004). Here, CWT is applied to spatial data and thus we refer to the wavelet domain as resolved both in scale and location. After the transformation, we applied an extension of wavelet analysis – wavelet coherence transform (WCT) (Maraun et al., 2007; Torrence and Webster, 1999) – to pairs of ferrybox data (CHLa fluorescence, PC fluorescence, turbidity) to resolve locations and scales of coherent variation.

Convolution of the signals with scaled and translated versions of the *mother-wavelet* was carried out in Fourier space, using discrete fast Fourier transform (DFFT). The finite length of the data sets would have caused edge effects when calculating the DFFT, which was mitigated by zero-padding the signal to a length of the next power of two. The effect of this procedure to the wavelet transform can be noticed within the *cone of influence* (COI). Outside the COI, discontinuities at the edges are contributing to the wavelet-transformed signal by less than a factor e^{-2} (two e-folding length), and can be considered negligible (Torrence and Compo, 1998). For the Morlet *mother-wavelet*, the two e-folding length at wavelet-scale s is $\sqrt{2}s$. Wavelet coherence was assumed significant if the coherence was higher, on the 95% significance level, than that between two random data sets with the same statistical properties. These red-noise data sets were calculated with Monte Carlo simulations, using an autoregressive AR1 model (Torrence and Compo, 1998).

All calculations were carried out according to the recommendations by Torrence and Compo (1998), with the routines described by Grinsted (2004), who also implemented the functionality as a freely available (non-profit use) Matlab (The Mathworks) module. The open-source package 'PiWavelet' (Pereira, 2014) offers an easy-to-use implementation of these routines for Python and is used here. For a full theoretical treatment of wavelet analysis we refer to Daubechies (1992).

2.3. Bloom detection and classification scheme

Wavelet coherence transforms (WCT) between all ferrybox parameter combinations (PC fluorescence and CHLa fluorescence: 'PC-CHLa coherence', CHLa fluorescence and turbidity: 'CHLa-turbidity coherence', PC fluorescence and turbidity: 'PC-turbidity coherence') were calculated and averaged over wavelet scales 40 to 60, which corresponds to distances of 20.2 to 64.0 km with a COI ranging from 57 to 85 km. For our data set, smaller scales tend to be affected by noise, whereas larger scales are spatially not sufficiently resolved to be useful in the context of bloom delineation. We note that the optimal range for the wavelet scale lies in the range where signal coherence can be detected, which needs not to bear relevance to the spatial extent of phytoplankton bloom. The bloom detection scheme is based only on the parameter combinations that include PC fluorescence, to ensure that cyanobacterial blooms rather than blooms of highly

scattering algae are detected. Significant PC-CHLa and PC-turbidity coherence, on the 95% significance level and at wavelet scales of 40–60 outside the COI, classify a potentially cyanobacteria dominated section ('cyano'). Wind speed and SST are used to delineate conditions that could lead to or indicate near-surface stratification along the ferrybox transects. Wind speeds ≥ 6 ms^{-1} are assumed to lead to mixed conditions ('mixed') even when strongly buoyant cells are present. Situations with wind speed ≤ 6 ms^{-1} are considered potentially stratified ('stratified'). If, in addition, SST exceeds the transect average by more than 0.75 °C, surface accumulations are likely ('floating'). In Section 4, we further elaborate on these specific choices and thresholds.

3. Results

We first present the temporal and spatial trends in the ferrybox, remote sensing and weather observations, followed by the results of the cyanobacterial bloom detection and stratification classification. In Section 3.3 we compare *in situ* and matching remote sensing observations for stratified and mixed bloom conditions.

3.1. Temporal and spatial trends

Relatively high average wind speeds were observed in the beginning and at the end of the study period, while low wind speed prevailed during the weeks in between (Fig. 2, top panel). SST increased from 15–18 °C at the start of the study period to 19–21 °C during mid-July, then decreased to 17–19 °C towards the end of July (Fig. 2, bottom panel).

Transect averages of ferrybox (IS) and remotely sensed (RS) variables are plotted for the study period in Fig. 3. PC peaked in early July, whereas CHLa (IS) shows relatively low values from early July through mid-July. An approximately inverse temporal relationship observed between CHLa (IS) and PC suggests that the community composition changed towards cyanobacterial dominance during July. CHLa (RS) and turbidity peaked mid-July. Water samples were collected along several transects and analyzed for CHLa concentration. These ranged from 2 ± 1 mg/m^3 during end of June to 6 ± 3 mg/m^3 early July and 5 ± 2 mg/m^3 during the second half of July.

The spatial distributions of the recorded CHLa fluorescence, PC fluorescence, turbidity and remotely sensed CHLa concentration are shown in Fig. 4. CHLa fluorescence was high in the area 800–950 km for the four transects sailed from 23 June to 1 July, henceforth referred to as 'late-June CHLa peak'. This peak is not apparent from PC fluorescence, turbidity or remotely sensed CHLa concentrations. The later transects do not show similar consecutive sections of high CHLa fluorescence, although the 13 and 25 July transects contain short sections of high fluorescence around 450–600 and 700–900 km from TravemÃ¼nde, respectively. PC fluorescence exhibited a very different distribution. The transects on 1 and 5 July show high PC fluorescence signals over the entire northern part, but infrequent high fluorescence in transects 11 until 17 July. Turbidity resembled the patterns observed in the PC fluorescence measurements. The highest remotely sensed CHLa concentrations (>115 mg/m^3) were observed in scenes 10, 11, 14 and 19 July.

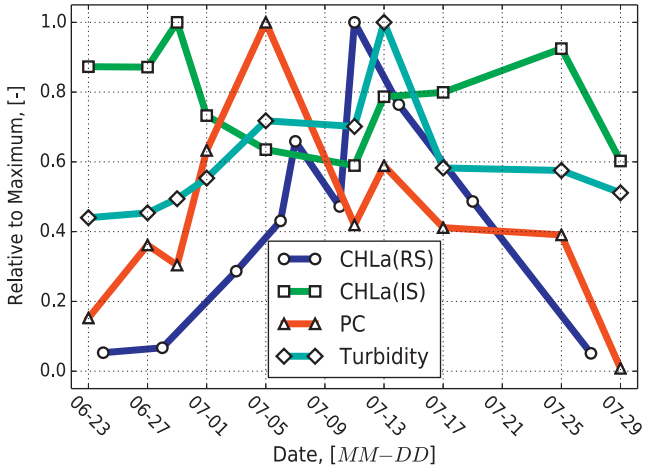

Fig. 3. Normalized transect averages of ferrybox *in situ* (IS) observations (CHLa fluorescence, PC fluorescence, turbidity) and CHLa concentrations from remote sensing (RS), plotted as a function of time.

3.2. Cyanobacterial bloom detection and classification

Fig. 5 shows the results of the wavelet coherence analysis for the *in situ* observations of CHLa fluorescence, PC fluorescence and turbidity along the transect in Fig. 1. All WCT plots show consecutive stretches of high coherence in the period of 5–25 July between approximately 350 and 950 km, with isolated sections of high coherence outside this area. Coherence close the edges of the transect, and therefore within the cone of influence (COI, ranging from 57 to 85 km from the edges), should be interpreted with care. For example, close to the harbor of Helsinki coherences are generally high, which might be caused by edge effects. In this particular case, however, CHLa (IS) and turbidity were both elevated, indicating high biomass. The COI areas are conservatively excluded from the bloom classification scheme in our analysis. In the supplement to this paper, the full scale information is given for each coherence product, which also includes the COI at each scale.

Fig. 6 depicts the result of the bloom classification scheme (see Section 2.3), applied to the coherence transforms from all transects outside of the COI. Transects from 5 to 25 July were classified as 'cyano' from approximately 350 to 950 km distance and predominantly flagged as 'stratified' or 'floating'. Outside this area, very few and short sections were classified as cyanobacteria dominated. Transect 13 July was flagged as 'mixed' from approximately 350 to 600 km with a subsequent stretch of floating cyanobacteria from approximately 650 to 800 km. Transect 11 July was also marked as floating from approximately 675 to 850 km.

3.3. Correlation between in situ and remote sensing observations

Multiple linear (generalized least squares) regression of remotely sensed CHLa concentrations against *in situ* observations (CHLa fluorescence, PC fluorescence, turbidity) was carried out for various subsets (Table 1). Only data sets collected when the satellite overpass was concurrent with ferrybox observations were evaluated. Four matching data sets are indicated with black lines in Fig. 2. M/S *Finnpartner* sailed the distance of 1091 km in typically 30 h, resulting in a maximal time difference of 22 h between the observations. The correlations for unmasked transects ('all') were stronger for the pre-bloom scenes 6 and 28 June than for the bloom scenes 6 and 14 July. Subsets characterized as 'mixed' consistently yielded higher coefficients of determination (R^2) than stratified subsets. Similarly, sections characterized as 'non-cyano' show stronger correlations than cyanobacteria-dominated sections. By excluding stratified (including floating) cyanobacteria dominated sections from the analysis ('non-(cyano + strat)'), R^2 for all match-ups either remained constant or improved by up to 0.32 (14 July).

The match-up of transect 13 July with the remote sensing scene 14 July stands out in the result set because this scene captured the bloom peak and allows comparison of mixed and stratified conditions. A summary of all available information for this match-up is given in Fig. 7. In sections marked as 'mixed', increased remote sensing concentrations are resembled by elevated *in situ* observations at 5 m depth. In contrast, the stratified section between approximately 650 and 750 km exhibited exceptionally high remotely sensed concentrations, which are not evident from *in situ* observations. This is reflected by stronger correlations for mixed (Table 1, $R^2 = 0.66$, N = 2668) than for stratified observations ($R^2 = 0.37$, N = 4751), suggesting that ship-induced mixing

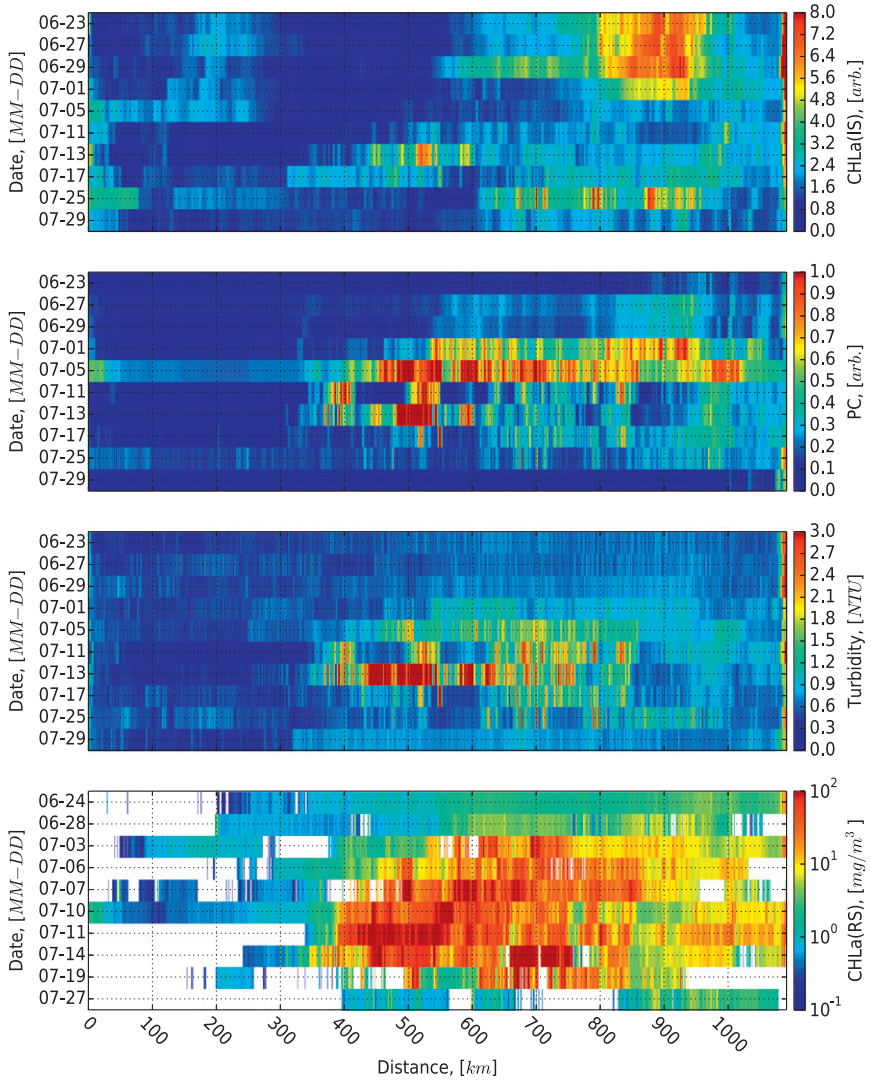

Fig. 4. Measurements of ferrybox (IS) CHLa fluorescence, PC fluorescence, turbidity and remote sensing (RS) CHLa concentration. All measurements were collected along the transect in Fig. 1. See Fig. 2 for further information on distance and dates.

was not able to overcome stratification. However, regardless of the stratification situation, all wavelet coherence products indicate cyanobacteria dominated observations. The subset marked as cyanobacteria dominated is weakly correlated ($R^2 = 0.09$, N = 2930), which is explained by a weak correlation in the subset of stratified observations ($R^2 = 0.08$, N = 1257), whereas the wind-mixed subset renders an R^2 of 0.55 (N = 1673). Consequently, when the stratified cyanobacteria dominated subset is excluded, the overall correlation increases from $R^2 = 0.36$ to $R^2 = 0.68$. An exclusion of all cyanobacteria dominated observations increases R^2 only to 0.61.

4. Discussion

4.1. Contradicting ferrybox and remote sensing observations

In situ fluorescence of CHLa and PC as well as remote sensing derived CHLa concentrations are widely used for bloom detection and trend analysis (Fleming and Kaitala, 2006; Frank et al., 2010) (Kutser, 2009; Matthews et al., 2010). All these parameters are expected to be positively correlated with bloom development. However, each of the trends in Fig. 3 leads to a different conclusion about bloom development status. Two factors hamper a consistent evaluation: 1) PC fluorescence increased with the bloom development, while CHLa fluorescence decreased, and 2) PC fluorescence and remotely sensed CHLa concentrations did not reach their peak values at the same time.

An explanation for 1) may be the different sources of pigment fluorescence between algae and cyanobacteria. In cyanobacteria, a significantly lower fraction of cellular CHLa is connected to the fluorescing photosystem II compared to algae (Johnsen and Sakshaug, 1996). This leads to a lower fluorescence response from the CHLa fluoroprobe when cyanobacteria become dominant. At the same time, PC fluorescence will increase with increasing cyanobacteria dominance, at least under nutrient replete conditions (i.e., during bloom development). Consistently, Seppälä et al. (2007) found that the variability in extracted CHLa pigment concentration is better explained by PC and CHLa fluorescence trends than CHLa fluorescence alone when cyanobacterial dominance increases.

We interpret 2), the time-delay between ferrybox and remote sensing observations, as the time that the cyanobacterial bloom needs from its initiation until formation of large-scale stratified patches or even floating layers, when weather conditions allow. This supports the conclusion of Kanoshina et al. (2003) that first bloom phases are well captured by ferrybox systems at the sampling depth of 5 m, whereas later, potentially stratified phases are better resolved by remote sensing.

Despite the contrasting trends in the optical signals recorded from ferryboxes and remote sensing platforms, the approach presented in

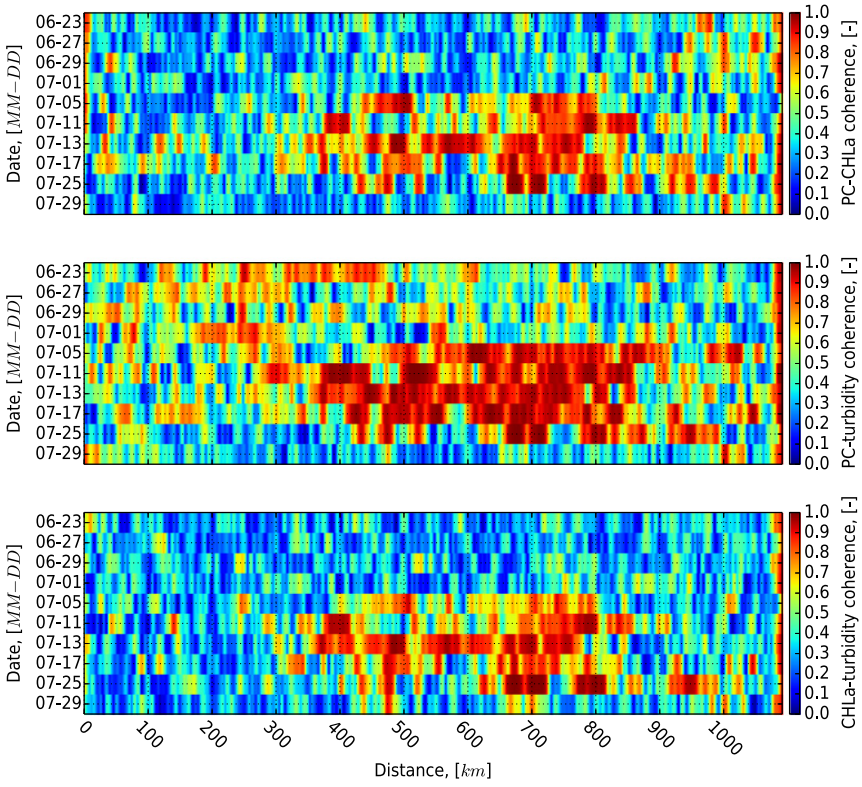

Fig. 5. Wavelet coherence between PC fluorescence and CHLa fluorescence (top panel), PC fluorescence and turbidity (middle panel) and CHLa fluorescence and turbidity (bottom panel) for all analyzed transects. Coherence on wavelet scales from 40 to 60 (corresponds to distances of 20.2 to 64.0 km) were averaged. The 95% significance level varies between 0.70 and 0.72 for all of these scales. See Fig. 2 for further information on distance and dates.

this paper allows for a corroborative interpretation of these observations with complementary meteorological data.

4.2. Cyanobacterial bloom detection and classification

Our classification of bloom sections as mixed, stratified, or floating depends on thresholds for wind speed and SST. Wind velocities varying from 4 to 7.7 ms^{-1}, have been reported to cause sufficient vertical mixing of the water column in various studies (George and Edwards, 1976; Hunter et al., 2008; Wynne et al., 2010). For the purpose of our classification, mixing down to the measurement depth of the ferrybox system is sufficient. For SST, Kahru et al. (1993) explain that cyanobacteria can contribute to heating of the sea surface up to 1.5 °C. Suitable thresholds for wind speed and SST were selected based on these published observations and visual inspection of the classification results. We adopted the threshold of 6 ms^{-1} from Hunter et al. (2008) for *Microcystis aeruginosa* in a eutrophic shallow lake, considered appropriate for buoyant filamentous cyanobacteria in the thermally stratified Baltic Sea. The threshold for SST leading to a classification as 'floating' was set at 0.75 °C elevation over the transect average. In some cases, a threshold definition based on a global transect mean is problematic, for example in mid-July transects when SST was high throughout the transect (see Fig. 2). Operationally, a dynamic threshold could be determined from multi-year climatologies or sufficiently resolved hydrodynamic models. SST anomalies (difference between day- and night-time SSTs) could also be derived from geostationary satellites, as recently demonstrated for the Baltic Sea by Karagali et al. (2012).

The resolution of the SST and wind speed data was relatively coarse compared to the ferrybox and satellite data. Meteorological data of higher spatial and temporal resolution could offer more detailed insights into bloom structure and development. The global, near-real-time and free-of-charge availability of ECMWF proved sufficiently resolved for the purpose of interpreting multi-source optical data in this study. A 'pixel-wise' classification of floating vegetation using spectral reflectance properties (e.g. Matthews et al., 2012) could complement this method.

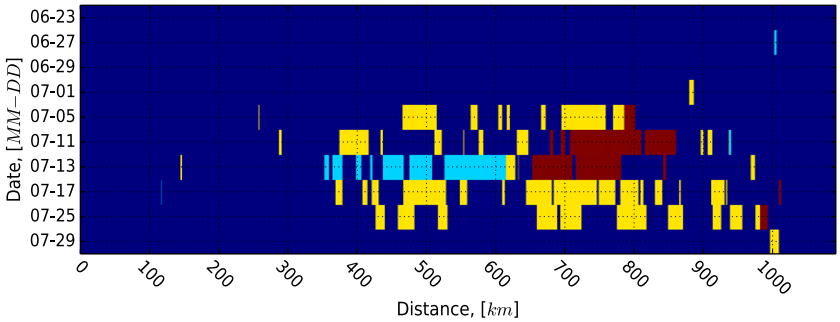

Fig. 6. Bloom classification. Stratification conditions are marked as: mixed (light blue), stratified (yellow) and floating (red). Flags within the cone of influence (COI, see Section 2.2) are omitted. See Fig. 2 for further information on distance and dates.

Table 1
Coefficients of determination (R^2) from a multiple regression (generalized least squares) of remotely sensed CHLa against *in situ* observations (CHLa fluorescence, PC fluorescence, turbidity) for all match-ups. The first row indicates the dates of satellite overpass (MM-DD in 2005). Fig. 2 shows match-up times and locations. Different masks were applied: 'all' (no mask), 'mixed' (only vertically mixed water columns), 'strat' (only stratified or floating conditions), 'cyano' (only sections classified as cyanobacteria dominated), and combinations thereof. In parentheses, the number of observations for each mask is indicated. The p-value of the F-statistics for all correlations is <0.05.

	06-24	06-28	07-06	07-14
All	0.63 (8066)	0.55 (7365)	0.48 (6891)	0.36 (7419)
Mixed	0.79 (3458)	0.70 (3691)	–	0.66 (2668)
Strat	0.66 (4608)	0.38 (3674)	0.48 (6891)	0.37 (4751)
Cyano	0.44 (127)	0.53 (32)	0.17 (1403)	0.09 (2930)
Non-cyano	0.81 (7939)	0.55 (7333)	0.48 (5488)	0.61 (4489)
Cyano + mixed	–	0.53 (32)	–	0.55 (1673)
Cyano + strat	0.44 (127)	–	0.17 (1403)	0.08 (1257)
Non-(cyano + strat)	0.81 (7939)	0.55 (7365)	0.48 (5488)	0.68 (6162)

The spatial resolution of the current analysis is determined by the coherence analysis. Coherence at very small scales, and thus distances, tends to be erratic (see full coherence graphs provided in the supplement). We were not able to find consistent coherent variation at very small scales (e.g. < 20 km). We can speculate about the causes for this distinct scaling behavior. One possible reason might be that at very small scales instrument noise plays a dominant role. It might also be the case that small-scale structures are masked by ship-induced mixing and water transport from the intake to the instruments. Consequently, we excluded coherence at wavelet scales corresponding to distances smaller than 20 km. Coherence on very large scales (e.g. > 64 km), in turn, were excluded because they do not allow to delineate cyanobacteria dominated subsections. However, it is very likely that coherence on other scales and ratios thereof can offer additional information about underlying biogeochemical processes, such as typical bloom structure sizes or phytoplankton group composition.

Conventional bloom metrics are based on regionally established threshold values (e.g. Metsamaa et al., 2006), which can lead to misleading interpretations at highly stratified conditions. We introduce the concept of significant coherence between independent *in situ* optical transect measurements as a different criterion for cyanobacterial blooms. Each coherence product comes with its own interpretation: 1) PC-CHLa coherence implies that sample-to-sample variation in phytoplankton biomass (CHLa fluorescence) corresponds to the variation in cyanobacterial accessory photosynthetic pigment (PC fluorescence), which is increasingly likely with increasing cyanobacteria dominance. Similar to the previous, 2) PC-turbidity coherence indicates that a dominant cyanobacteria presence exists. This is provided that the particle population does not include significantly variable, highly scattering, non-cyanobacterial components. Positively buoyant cyanobacteria are frequently considered efficient light scatterers either due to the presence of gas vacuoles or colony formation. Based on this, PC-turbidity coherence is likely to indicate bloom-forming cyanobacteria. Finally, 3) CHLa-turbidity coherence should be interpreted as the dominant presence of phytoplankton in the particle population. For turbidity sensors with limited signal resolution, this product is more likely to be significant when the dominant phytoplankton is an efficient light scatterer.

Seppälä et al. (2007) reported the presence of *Anabaena* spp., *Aphanizomenon flos-aquae* and *N. spumigena* in the studied period, all of which were found to be efficient light scatterers (Metsamaa et al., 2006). This suggests that high coherence in all three products was caused by abundant cyanobacteria. Turbidity originating from other scattering substances, e.g. suspended matter and sea water, is not expected to be coherent with the fluorescence signals. Variability induced by e.g. suspended matter might however decrease the level of coherence between turbidity and fluorescence measurements to below the applied 95% significance threshold for wavelet coherence. In our data set, PC-turbidity coherence and CHLa-turbidity coherence were similar or even stronger than PC-CHLa coherence, suggesting that scattering was indeed dominated by cyanobacteria.

Elevated CHLa fluorescence (Fig. 4) in the northern parts of the late June transects ('late-June CHLa peak') coincided with high wind-forced mixing (Fig. 2). Fluorescence measured at 5 m depth should therefore be representative of the remotely sensed concentration in the first optical depth during this period. Surprisingly, the remote sensing derived CHLa concentrations were not elevated despite the suggestion of phytoplankton bloom from the CHLa fluorescence in this area. The late-June CHLa peak is also not apparent from the ferrybox turbidity measurements, suggesting that the source of the CHLa fluorescence peak was a weak light scatterer.

Low light scattering efficiency in visible wavebands by small flagellates is consistent with results from Steen (2004) on *Chrysochromulina ericina*. This explanation, and the general correspondence between the WeW/FUB CHLa concentrations and turbidity measurements at 5 m depth, suggest that the WeW/FUB CHLa algorithm is more sensitive to increased scattering by certain phytoplankton species than to the specific absorption features of the CHLa pigment. The late-June CHLa peak is also not visible in any of the coherence products. This supports our conclusion that PC-turbidity and PC-CHLa coherence are not sensitive to algal blooms but specifically to cyanobacterial blooms. However, our data set does not allow us to verify whether CHLa-turbidity coherence is also sensitive to non-cyanobacterial, strongly scattering phytoplankton. We recommend to test the approach on additional data sets that would capture the occurrence of such species, e.g. from Baltic Sea spring blooms. Similarly, phycocyanin-poor cyanobacteria such as marine Synechococcus sp. or the phycocyanin-lacking prochlorophytes may not be distinguished with the same set of fluorescence parameters.

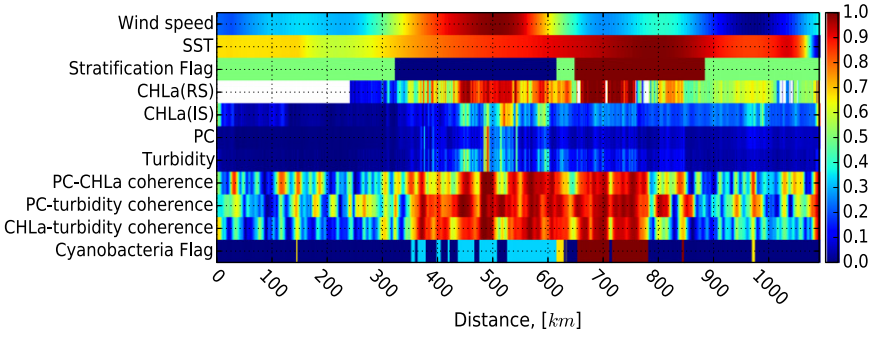

Fig. 7. Combined graph of all data sources (IS: *in situ*, RS: remote sensing) for transect 07-13 and the matching remote sensing scene 07-14. Each parameter is normalized to its respective minimum and maximum values. For the 'Stratification Flag', stratification conditions are marked as: mixed (blue), stratified (green) and floating (red). For the 'Cyanobacteria Flag', stratification conditions are marked as: mixed (light blue), stratified (yellow) and floating (red). See Fig. 2 for further information on distance and dates.

Based on the 2005 bloom description given by Seppälä et al. (2007) we conclude that wavelet coherence successfully delineates the spatial and temporal extent of the analyzed cyanobacterial bloom. We observed significant coherence in mixed, stratified and even surface bloom subsections (e.g. 11 July, ≈700–850 km and 13 July, ≈650–800 km)—independent of the corresponding fluorescence or turbidity signal strength. Within the resolution limits of the stratification classification, we conclude that wavelet coherence between ferrybox measurements appears to be largely independent of concentration and thus stratification. Further research is however necessary to quantify the relationship between the level of coherence and absolute pigment concentrations, community composition, and the presence of other particulate matter.

4.3. Correlation between ferrybox and remote sensing observations

Fig. 7 illustrates a situation where remote sensing and *in situ* observations do not match. The subsection of the 13 July transect marked as floating bloom (≈650–800 km) could not be detected using only magnitudes of the measured *in situ* signals. Exceptionally high remotely sensed CHLa concentrations, low wind speed and high SST make the presence of surfacing cyanobacteria patches very likely. Several remotely sensed pixels within that patch are indeed flagged as 'floating vegetation', according to the definition of Matthews et al. (2012) (results not shown). This interpretation is reflected by the automatically produced 'Cyanobacteria Flag' in Figs. 6 and 7. By excluding stratified and floating cyanobacteria dominated sections, the correlation between *in situ* and remotely sensed observations could be increased significantly (from $R^2 = 0.36$ to 0.68 for scene 14 July, Table 1). In this case, only 17% of the observations had to be masked to achieve this result. The difference in correlation between stratified and mixed cyanobacteria dominated sections ($R^2 = 0.08$ and 0.55) indicates that only the latter are suitable for comparison with remotely sensed concentration estimates. The correlation for the remaining match-up scenes is also either unaffected or improved by the masking.

It may be argued that large cargo ships and passenger ferries mix the water column sufficiently to avoid effects from stratification in ferrybox measurements (Rantajärvi et al., 1998). Our findings suggest that in highly stratified conditions up to surfacing blooms, ship-induced mixing might not be sufficient to avoid discrepancies between remote sensing and *in situ* observations. Such discrepancies may be caused by incomplete mixing or lingering cell physiological effects of light exposure on pigment production and fluorescence. We recommend to exclude observations of stratified or floating cyanobacterial blooms in the direct comparison of ferrybox and optical remote sensing data. Mixed bloom sections should be explicitly included, as they represent the upper reliably observable concentration limits. If data assimilation is desired, we recommend to anticipate and interpret deviations between the observation sources according to the presented scheme.

4.4. Implications for the Baltic Sea

In the Baltic Sea *in situ* observations are carried out routinely from ships-of-opportunity, buoys, research vessels, and increasingly by citizens. It is challenging to combine these observations into a comprehensive monitoring network. This problem born out of luxury makes automatic interpretation of data from operational sensor networks essential: near real-time data access is reduced to a technical detail if interpretation and evaluation cannot be carried out at the same pace. Decision making processes, e.g. harmful-algae early warning systems, require near real-time interpretation and harmonization of the diverse data sources. The approach presented in this study is one answer to this requirement. It is particularly useful in the context of Baltic Sea ferryboxes, because these systems resolve three independent measures of cyanobacterial presence: fluorescence of CHLa and PC as well as turbidity. We found coherence between these observations to be high throughout cyanobacteria dominated water bodies, independent of the actual cell abundance at the measurement depth. This makes the detection less sensitive to wind mixing or cell migration. The presented method assimilates these coherences, along with wind speed and SST, to a synoptic product of cyanobacterial bloom presence and stratification status, and can be readily applied in near real-time data analysis.

5. Conclusion

Using ferrybox instruments and weather data, a harmonized cyanobacterial bloom presence and qualification method was developed. Coherent *in situ* measurements are interpreted as driven by the same source—cyanobacterial cells. Wavelet coherence analysis was applied to spatially resolve this coherence. Combinations of PC fluorescence, CHLa fluorescence, and turbidity vary coherently in a cyanobacteria dominated bloom in the Central Baltic Sea. Coherence was found to be significant at all encountered levels of stratification. In highly stratified conditions, e.g. at low wind speed and elevated sea surface temperature, coherent observations indicate where surface accumulations will highly affect remote sensing measurements while ferrybox-derived concentrations of PC and especially CHLa can be rather low. In well-mixed cyanobacteria dominated blooms, concentrations derived from space and *in situ* can be compared directly. Both conditions can automatically be identified with the developed approach, which is a precursor to near-real time processing efforts and further data assimilation. We demonstrated that resolving coherence between independent ferrybox measurements supports corroborative interpretation of multi-platform cyanobacterial bloom observations. Thus we recommend that ferrybox systems operated in regions of abundant cyanobacteria be equipped with CHLa and PC fluorometers as well as turbidity sensors. Also wind speed should be among the recorded parametersin ferrybox systems to facilitate near real-time processing. The approach might be particularly valuable for automated cyanobacteria monitoring and early warning systems.

Acknowledgments

We acknowledge the Alg@line consortium and those researchers who took the initiative for phycocyanin measurements, in particular Jukka Seppälä and Pasi Ylöstalo from FIMR (presently SYKE). The authors are grateful to the European Space Agency for the MERIS imagery and to ECMWF for the meteorological data. PMMG and SGHS received support from EC/IAPP project WaterS (Grant 251527), MAE and SWMP were co-funded by the European Community Seventh Framework Programme under grant agreement nr. 263295 CoBiOS.

Appendix A. Supplementary data

Supplementary data to this article can be found online at http://dx.doi.org/10.1016/j.jmarsys.2014.05.015.

References

Ampe, E.M., Hestir, E.L., Bresciani, M., Salvadore, E., Brando, V.E., Dekker, A., Malthus, T.J., Jansen, M., Triest, L., Batelaan, O., 2013. A wavelet approach for estimating chlorophyll-a from inland waters with reflectance spectroscopy. IEEE Geosci. Remote Sens. Lett. 1–5.

Anderson, D., 1997. Turning back the harmful red tide. Nature 388, 513–514.

Anderson, D., Glibert, P., Burkholder, J., 2002. Harmful algal blooms and eutrophication: nutrient sources, composition, and consequences. Estuaries 25, 704–726.

Blauw, A.N., Benincà, E., Laane, R.W.P.M., Greenwood, N., Huisman, J., 2012. Dancing with the tides: fluctuations of coastal phytoplankton orchestrated by different oscillatory modes of the tidal cycle. PLoS One 7, e49319.

Campbell, D., Hurry, V., 1998. Chlorophyll fluorescence analysis of cyanobacterial photosynthesis and acclimation. Microbiol. Mol. Biol. Rev. 62, 667–683.

Carstensen, J., Conley, D., Henriksen, P., 2004. Frequency, composition, and causes of summer phytoplankton blooms in a shallow coastal ecosystem, the Kattegat. Limnol. Oceanogr. 49, 191–201.

Daubechies, I., 1992. Ten lectures on wavelets. CBMS-NSF Regional Conference Series in Applied Mathematics. SIAM: Society for Industrial and Applied Mathematics.

Dee, D.P., Uppala, S.M., Simmons, a.J., Berrisford, P., Poli, P., Kobayashi, S., Andrae, U., Balmaseda, M.a., Balsamo, G., Bauer, P., Bechtold, P., Beljaars, a.C.M., van de Berg, L., Bidlot, J., Bormann, N., Delsol, C., Dragani, R., Fuentes, M., Geer, a.J., Haimberger, L., Healy, S.B., Hersbach, H., Hólm, E.V., Isaksen, L., Kå llberg, P., Köhler, M., Matricardi, M., McNally, a.P., Monge-Sanz, B.M., Morcrette, J.J., Park, B.K., Peubey, C., de Rosnay, P., Tavolato, C., Thépaut, J.N., Vitart, F., 2011. The ERA-Interim reanalysis: configuration and performance of the data assimilation system. Q. J. R. Meteorol. Soc. 137, 553–597.

Fleming, V., Kaitala, S., 2006. Phytoplankton spring bloom intensity index for the Baltic Sea estimated for the years 1992 to 2004. Hydrobiologia 554, 57–65.

Frank, C., Schroeder, F., Petersen, W., 2010. FerryBox: using automated water measurement systems to monitor water quality: perspectives for the Yangtze river and Three Gorges Dam. J. Earth Sci. 21, 861–869.

George, D., Edwards, R., 1976. The effect of wind on the distribution of chlorophyll a and crustacean plankton in a shallow eutrophic reservoir. J. Appl. Ecol. 13, 667–690.

Gnanadesikan, A., Anderson, W.G., 2009. Ocean water clarity and the ocean general circulation in a coupled climate model. J. Phys. Oceanogr. 39, 314–332.

Gordon, H.R., McCluney, W.R., 1974. Estimation of the depth of sunlight penetration in the sea for remote sensing. Appl. Opt. 1, 413–416.

Grinsted, A., 2004. Application of the cross wavelet transform and wavelet coherence to geophysical time series. Nonlinear Process. Geophys. 11, 561–566.

Hallegraeff, G.M., 1993. A review of harmful algal blooms and their apparent global increase. Phycologia 32, 79–99.

Hansson, M., Hakansson, B., 2007. The Baltic Algae Watch System—a remote sensing application for monitoring cyanobacterial blooms in the Baltic Sea. J. Appl. Remote. Sens. 1, 011507.

Heisler, J., Glibert, P., Burkholder, J., Anderson, D., Cochlan, W., Dennison, W., Dortch, Q., Gobler, C., Heil, C., Humphries, E., Lewitus, a., Magnien, R., Marshall, H., Sellner, K., Stockwell, D., Stoecker, D., Suddleson, M., 2008. Eutrophication and harmful algal blooms: a scientific consensus. Harmful Algae 8, 3–13.

Hunter, P.D., Tyler, A.N., Willby, N.J., Gilvear, D.J., 2008. The spatial dynamics of vertical migration by Microcystis aeruginosa in a eutrophic shallow lake: A case study using high spatial resolution time-series airborne remote sensing. Limnol. Oceanogr. 53, 2391–2406.

Johnsen, G., Sakshaug, E., 1996. Light harvesting in bloom-forming marine phytoplankton: species-specificity and photoacclimation. Sci. Mar. 60, 47–56.

Kahru, M., Leppänen, J., Rud, O., 1993. Cyanobacterial blooms cause heating of the sea surface. Mar. Ecol. Prog. Ser. 101, 1–7.

Kahru, M., Savchuk, O., Elmgren, R., 2007. Satellite measurements of cyanobacterial bloom frequency in the Baltic Sea: interannual and spatial variability. Mar. Ecol. Prog. Ser. 343, 15–23.

Kanoshina, I., Lips, U., Leppänen, J.M., 2003. The influence of weather conditions (temperature and wind) on cyanobacterial bloom development in the Gulf of Finland (Baltic Sea). Harmful Algae 2, 29–41.

Karagali, I., Hø yer, J., Hasager, C., 2012. SST diurnal variability in the North Sea and the Baltic Sea. Remote Sens. Environ. 121, 159–170.

Kiefer, D.A., 1973. Fluorescence properties of natural phytoplankton populations. Mar. Biol. 22, 263–269.

Kratzer, S., Brockmann, C., Moore, G., 2008. Using MERIS full resolution data to monitor coastal waters—a case study from Himmerfjärden, a fjord-like bay in the northwestern Baltic Sea. Remote Sens. Environ. 112, 2284–2300.

Kutser, T., 2009. Passive optical remote sensing of cyanobacteria and other intense phytoplankton blooms in coastal and inland waters. Int. J. Remote Sens. 30, 4401–4425.

Kutser, T., Metsamaa, L., Dekker, A.G., 2008. Influence of the vertical distribution of cyanobacteria in the water column on the remote sensing signal. Estuar. Coast. Shelf Sci. 78, 649–654.

Leppänen, J.M., Rantajärvi, E., Maunumaa, M., Larinmaa, M., Pajala, J., 1994. Unattended algal monitoring system—a high resolution method for detection of phytoplankton blooms in the Baltic Sea. Proceedings of OCEANS94, pp. 461–463.

Maraun, D., Kurths, J., 2004. Cross wavelet analysis: significance testing and pitfalls. Nonlinear Process. Geophys. 11, 505–514.

Maraun, D., Kurths, J., Holschneider, M., 2007. Nonstationary Gaussian processes in wavelet domain: synthesis, estimation, and significance testing. Phys. Rev. E. 75, 016707.

Matthews, M.W., Bernard, S., Winter, K., 2010. Remote sensing of cyanobacteria-dominant algal blooms and water quality parameters in Zeekoevlei, a small hypertrophic lake, using MERIS. Remote Sens. Environ. 114, 2070–2087.

Matthews, M.W., Bernard, S., Robertson, L., 2012. An algorithm for detecting trophic status (chlorophyll-a), cyanobacterial-dominance, surface scums and floating vegetation in inland and coastal waters. Remote Sens. Environ. 124, 637–652.

Metsamaa, L., Kutser, T., Strombeck, N., 2006. Recognising cyanobacterial blooms based on their optical signature: a modelling study. Boreal Environ. Res. 11, 493–506.

Paerl, H.W., Huisman, J., 2009. Climate change: a catalyst for global expansion of harmful cyanobacterial blooms. Environ. Microbiol. Rep. 1, 27–37.

Pereira, E.S., 2014. PiWavelet.

Pulliainen, J., Vepsäläinen, J., Kaitala, S., Hallikainen, M., Kallio, K., Fleming, V., Maunula, P., 2004. Regional water quality mapping through the assimilation of spaceborne remote sensing data to ship-based transect observations. J. Geophys. Res. 109, 1–11.

Rantajärvi, E., Olsonen, R., Hällfors, S., Leppänen, J.M., Raateoja, M., 1998. Effect of sampling frequency on detection of natural variability in phytoplankton: unattended high-frequency measurements on board ferries in the Baltic Sea. ICES J. Mar. Sci. 55, 697–704.

Rantajärvi, E., Flinkman, J., Ruokanen, L., Hällfors, S., Stipa, T., Suominen, T., Kaitala, S., Maunula, P., Fleming, V., Lips, U., London, L., Vepsäläinen, J., Nyman, E., Neuvonen, S., Suominen, T., Kankaanpää, H., Seppälä, J., Perttilä, M., Raateoja, M., Haahti, H., 2003. Alg@line in 2003: 10 years of innovative plankton monitoring and research an operational information service in the Baltic Sea. Technical Report. Finnish Institute of Marine Research.

Ruokanen, L., Kaitala, S., Flemming, V., Maunula, P., 2003. Alg@line: joint operational unattended phytoplankton monitoring in the Baltic Sea. Elsevier Oceanogr. 69, 519–522.

Schroeder, T., Behnert, I., 2007. Atmospheric correction algorithm for MERIS above case-2 waters. Int. J. Remote Sens. 28, 1469–1486.

Schroeder, T., Schaale, M., Fischer, J., 2007. Retrieval of atmospheric and oceanic properties from MERIS measurements: a new case-2 water processor for BEAM. Int. J. Remote Sens. 28, 5627–5632.

Seppälä, J., Ylöstalo, P., Kaitala, S., Hällfors, S., Raateoja, M., Maunula, P., 2007. Ship-of-opportunity based phycocyanin fluorescence monitoring of the filamentous cyanobacteria bloom dynamics in the Baltic Sea. Estuar. Coast. Shelf Sci. 73, 489–500.

Steen, H.B., 2004. Flow cytometer for measurement of the light scattering of viral and other submicroscopic particles. Cytometry A 57, 94–99.

Stelzer, K., Geiß ler, J., Brockmann, C., Klein, H., Göbel, J., Reinart, A., Sø rensen, K., 2008. MERIS validation with respect to operational monitoring. Proc. of the 2nd MERIS/(A)ATSR User Workshop, pp. 3–7.

Torrence, C., Compo, G., 1998. A practical guide to wavelet analysis. Bull. Am. Meteorol. Soc. 79, 61–78.

Torrence, C., Webster, P., 1999. Interdecadal changes in the ENSO-monsoon system. J. Clim. 12, 2679–2690.

Vepsäläinen, J., Pyhälahti, T., Rantajärvi, E., Kallio, K., Pertola, S., Stipa, T., Kiirikki, M., Pulliainen, J., Seppälä, J., 2005. The combined use of optical remote sensing data and unattended flow-through fluorometer measurements in the Baltic Sea. Int. J. Remote Sens. 26, 261–282.

Walsby, A.E., Hayes, P.K., Boje, R., Stal, L.J., 1997. The selective advantage of buoyancy provided by gas vesicles for planktonic cyanobacteria in the Baltic Sea. New Phytol. 136, 407–417.

Wynne, T.T., Stumpf, R.P., Tomlinson, M.C., Dyble, J., 2010. Characterizing a cyanobacterial bloom in Western Lake Erie using satellite imagery and meteorological data. Limnol. Oceanogr. 55, 2025–2036.